Science of the Total Environment 935 (2024) 173252

Contents lists available at ScienceDirect

Science of the Total Environment

journal homepage: www.elsevier.com/locate/scitotenv

Numerical modeling of PFAS movement through the vadose zone: Influence of plant water uptake and soil organic carbon distribution

Barbara Jennifer Biesek [a,*], Adam Szymkiewicz [a], Jirka Šimůnek [b], Anna Gumuła-Kawęcka [a], Beata Jaworska-Szulc [a]

[a] Gdańsk University of Technology, Faculty of Civil and Environmental Engineering, ul. Gabriela Narutowicza 11/12, 80-233 Gdańsk, Poland
[b] Department of Environmental Sciences, University of California Riverside, Riverside, CA, USA

HIGHLIGHTS

- Use of organic carbon data from top soil layers overestimates PFAS travel time.
- Root zone slows down PFAS travel time due to transpiration.
- Root zone increases PFAS concentrations in soil water.
- Influence of root zone on PFAS movement is more important in fine soils.
- Root water uptake leads to increase of PFAS accumulation on Air Water Interface Area.

GRAPHICAL ABSTRACT

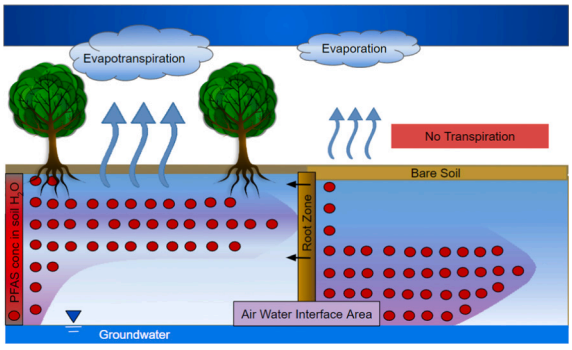

ARTICLE INFO

Editor: Damià Barceló

Keywords:
PFAS
HYDRUS
Root water uptake
Soil organic carbon
Soil contamination
Clean water and sanitation

ABSTRACT

In this study, we investigated the effects of soil organic carbon (SOC) distribution and water uptake by plant roots on PFAS movement in the vadose zone with a deep groundwater table under temperate, humid climate conditions. Two series of numerical simulations were performed with the HYDRUS computer code, representing the leaching of historical PFOS contamination and the infiltration of water contaminated with PFOA, respectively. We considered soil profiles with three distributions of SOC (no SOC, realistic SOC distribution decreasing with depth, and uniform SOC equal to the content measured in topsoil), three root distributions (bare soil, grassland, and forest), and three soil textures (sand, sandy loam, and loam). The SOC distribution had a profound impact on the velocity of PFOS movement. The apparent retardation factor for realistic SOC distribution was twice as large as for the scenario with no SOC and more than three times smaller than for the scenario with uniformly high SOC content. We also showed that the root distribution in soil profoundly impacts the simulations of PFAS migration through soil. Including the root zone significantly slows down the movement of PFAS, primarily due to increased evapotranspiration and reduced downward water flux. Another effect of water uptake by plant roots is an increase of PFAS concentrations in soil water (evapo-concentration). The evapo-concentration and the slowdown of PFAS movement due to root water uptake are more significant in fine-textured soils than in sand.

* Corresponding author.
E-mail address: bb2016@protonmail.com (B.J. Biesek).

https://doi.org/10.1016/j.scitotenv.2024.173252
Received 1 February 2024; Received in revised form 12 May 2024; Accepted 12 May 2024
Available online 18 May 2024
0048-9697/© 2024 The Authors. Published by Elsevier B.V. This is an open access article under the CC BY-NC-ND license (http://creativecommons.org/licenses/by-nc-nd/4.0/).

1. Introduction

The term PFAS refers to a group of over 15,000 *per-* and polyfluoroalkyl substances containing carbon fluorine bonds (US EPA, 2024). Large amounts of energy are required to break a single C—F bond, making it one of the strongest bonds in organic chemistry (Murphy et al., 2003). Possessing multiple C—F bonds is one of the characteristics that give PFAS their stability. The widespread use of PFAS in many industrial products and their resistance to environmental degradation make them one of the most important groups of contaminants worldwide. Although typically occurring in very low concentrations, they pose a considerable threat to human health. Increasing efforts are directed at monitoring PFAS presence and investigating their behavior in the environment. The soil compartment is particularly important since PFAS contamination typically originates at the ground surface, e.g., from the application of aqueous film-forming foams (AFFFs) for fire suppression, applications of biosolids, surface coating, de-icing components, and exposure to contaminated industrial waste (Sharifan et al., 2021; Minnesota Pollution Control Agency, 2024). PFAS are sorbed on soil particles and the air-water interface (AWI), potentially becoming a long-term groundwater contamination source. PFAS fate in soils is also affected by other factors, such as interactions with the microbiome and plant uptake (Sharifan et al., 2021).

Numerical models can be used to predict the fate of PFAS in soils and identify the main factors that control it (e.g., Zeng et al., 2021; Silva et al., 2022; Wallis et al., 2022). However, PFAS sorption on AWI depends on soil water content and cannot be represented by computer codes based on the standard transport equation (which typically includes advection, dispersion, and different models of sorption on solid). Until now, only a few numerical codes with the implementation of the AWI sorption mechanism have been reported in the literature and are publicly available. The well-known computer program HYDRUS (Šimůnek et al., 2008) based on the finite element method has been modified to include sorption on AWI, first in 1D and 2D (Silva et al., 2020) and later in the full 3D version of HYDRUS 5 (Šimůnek et al., 2023). Another numerical model was developed by Guo et al. (2020) for one dimension and later extended to three dimensions (Zeng and Guo, 2021). In this computer program equations describing water flow and PFAS transport are discretized using the cell-centered finite difference method and fully implicit first-order discretization in time. The resulting nonlinear equations are solved using Newton's iterative method. Wallis et al. (2022) added a simplified representation of AWI sorption to the LEACHM code (Hutson, 2003) describing 1D flow and transport in the soil profile. Furthermore, simplified analytical solutions for PFAS transport in the vadose zone were developed by Guo et al. (2022) and Smith et al. (2024). The above mentioned numerical and analytical models were applied to investigate the role of various factors influencing PFAS fate in vadose zone. Most applications focused on 1D vertical transport in laboratory columns (Silva et al., 2020; Zeng et al., 2021), in model (synthetic) soil profiles (e.g. Silva et al., 2020; Guo et al., 2020; Zeng et al., 2021) or in real soil profiles for which sufficient data were available (Silva et al., 2022; Wallis et al., 2022). So far, only few studies considered multidimensional flow (Zeng and Guo, 2021, 2023).

The AWI sorption of PFAS was described by equilibrium sorption isotherms: linear (e.g. Wallis et al., 2022) or Langmuir (e.g. Silva et al., 2020; Vahedian et al., 2024), as well as by kinetic sorption models. Guo et al. (2020) proposed a two-domain kinetic model for AWI sorption, where the equilibrium part was described by Langmuir isotherm, while the non-equilibrium part was described by a first-order kinetic model. This approach was followed in other studies (e.g. Zeng et al., 2021). Brusseau et al. (2021) concluded that linear equilibrium sorption models are good approximations if PFAS concentrations in water are 3 to 10 times lower than their critical concentrations, specific to each PFAS compound. The critical concentrations for two common PFAS compounds: PFOS and PFOA were reported as 1 mg/L and 10 mg/L, respectively (Brusseau et al., 2021). The adequacy of linear equilibrium sorption model was also shown by Zeng et al. (2021). Moreover, Brusseau et al. (2021) and Zeng et al. (2021) found kinetic effects in AWI sorption negligible for a wide range of conditions considered in their studies. Different approaches were also employed to calculate the AWI area, which is a key variable governing PFAS sorption. AWI area can be calculated from the water retention curve, based on the thermodynamic theory. This method was applied e.g. by Silva et al. (2020, 2022). In the absence of detailed data, Wallis et al. (2022) approximated AWI area as a linear function of water saturation. Laboratory measurements in soils suggest a nonlinear relationship between AWI area and water saturation, with measured AWI area for a specific saturation generally larger than the one obtained from thermodynamic method (e.g. Brusseau and Guo, 2021). A possible explanation for this discrepancy is the roughness of soil grains (Brusseau, 2023). Several studies used AWI – water saturation relationship obtained directly from measurements (e.g. Guo et al., 2020) or multiplied the AWI area obtained from the thermodynamic approach by an empirical scaling factor (e.g. Zeng et al., 2021). The sorption of PFAS at AWI modifies the air-water surface tension and capillary pressure in soil pores, leading to the so-called surfactant-induced flow. This effect was studied by Guo et al. (2020), Brusseau et al. (2021), Zeng and Guo (2021) and Vahedian et al. (2024).

PFAS sorption on solid phase is a complex process. It occurs on soil organic carbon (SOC), metal oxides and clay minerals and is affected by factors such as pH, cation exchange capacity and soil micropore volume (Li et al., 2018; Nguyen et al., 2020). In modeling studies sorption on solids is described using equilibrium models with linear isotherm (e.g. Wallis et al., 2022) or Freundlich isotherm (e.g. Zeng et al., 2021; Silva et al., 2022) or using kinetic models (e.g. Zeng et al., 2021). Zeng et al. (2021) found kinetic effects in solid sorption to be of minor importance for the field-relevant conditions examined in their study. Despite the complexity of PFAS sorption on solids, several authors used a simple linear model, which assumes a direct proportionality between the partition coefficient and the fraction of organic carbon in soils (e.g. Xiao et al., 2015; Wallis et al., 2022; Smith et al., 2024). This model can be easily parametrized and remains an attractive tool especially for screening calculations (e.g. Smith et al., 2024). However, the SOC distribution varies with depth. Typically, the maximum SOC concentration occurs near the surface and becomes very small below 2–3 m depth (Jobbágy and Jackson, 2000). SOC is often estimated in samples taken from the shallow soil layer. For example, Xiao et al. (2015) used the SOC fraction from shallow soil layers to estimate retardation factors for a contaminated site in Minnesota. Anderson (2021) noted that extrapolating estimates of SOC fraction from the shallow horizons through a whole soil profile may lead to unrealistic results. Only few studies accounted for the variability of solid sorption parameters with depth. Wallis et al. (2022) assumed a variable SOC distribution was assumed, based on soil sampling up to 7 m depth. The measured SOC profile was in good agreement with the average profiles reported by Jobbágy and Jackson (2000). Wallis et al. (2022) compared simulations with nonuniform SOC to simulations with no solid sorption and showed that sorption on solids leads to strong retention of PFAS within the shallow soil layer. Zeng and Guo (2023) used an extended linear sorption model, where the partitioning coefficient depended on both SOC and the content of clay and silt fraction (representing sorption on clay minerals). They assumed SOC distribution decreasing exponentially with depth, similar as in Jobbágy and Jackson (2000), which was constrained by the measured SOC at multiple depths. Smith et al. (2024) assumed a homogeneous vadose zone to apply analytical solutions, but the authors used a thickness-weighted average of the soil organic carbon content, which accounted for the fact that only a small fraction of SOC is present below the depth of 0.6 m. However, the potential error in PFAS movement prediction due to using SOC estimates from the top layer has not been quantified so far.

The relative importance of AWI and solid sorption for PFAS retention in soil varies with the soil texture, heterogeneity, solid sorption properties and climatic conditions. For example, Guo et al. (2020) presented

MOST WIEDZY Downloaded from mostwiedzy.pl

simulations of hypothetical PFAS transport scenarios in two soil types under typical humid and semi-arid climate. In their simulations, AWI sorption was the main mechanism for PFAS retention in the vadose zone, leading to retardation factors of the order from several hundred up to more than one thousand. The retention of PFAS at AWI was more significant in sand than in a soil with higher content of fine fractions. Silva et al. (2022) simulated PFAS leaching due to biosolids applications at two test sites in Illinois (US). In the considered scenarios, the effect of AWI sorption was much smaller than the sorption on solids due to relatively large water contents (and thus small air-water interfacial areas) in fine-textured soils. The same study also showed that AWI sorption was more important in a homogeneous silty sand profile than in a heterogeneous profile with several layers of fine-textured soils underlain by medium sand. This was consistent with earlier findings of Silva et al. (2020), who found that textural heterogeneities in 1D soil profile lead to faster downward movement of PFAS. In the studies of multidimensional transport by Zeng and Guo (2021, 2023) local textural heterogeneities were found to greatly impact PFAS movement, often leading to preferential transport much faster than predicted for homogeneous soil. Zeng and Guo (2023) identified reduction of the available AWI due to increasing water content in preferential flowpaths as the main mechanism accelerating movement of long-chain PFAS, such as PFOS, in heterogeneous soil.

Zeng et al. (2021) investigated PFAS leaching in hypothetical 4 m deep soil profiles in humid and semi-arid climates using realistic sets of daily weather data. They performed a comprehensive study of the model sensitivity with respect to several parameters. It was shown that the rank of the most sensitive parameters depends on the relative importance of solid-phase sorption vs. AWI sorption, which in turn depends on the PFAS chain length and applied concentrations. For two common compounds, PFOA and PFOS, the most sensitive parameters included dispersivity, the parameter alpha in the van Genuchten retention function (which additionally influences the calculated AWI area), saturated water content, parameters describing AWI properties, and the exponent in the Freundlich isotherm representing sorption on solids.

Until now, relatively little attention has been paid to the role of water uptake by plant roots in the transport of PFAS. The presence of roots modifies flow velocities and water contents, and consequently also AWI areas in the soil profile. Wallis et al. (2022) seem to be the only study that included the root zone in a PFAS transport model. They simulated PFAS transport in a 7 m deep vadose zone profile in Australia, based on data obtained from a site affected by historical AFFF application. Wallis et al. (2022) considered seasonal growth of grass cover at the site, with varying root depth (up to 30 cm) and including the effect of plant growth on evapotranspiration. They showed a significant role of PFAS evapoconcentration in the upper part of the soil profile, i.e., an increase in PFAS concentrations due to evapotranspiration of water from the soil (their model did not include PFAS uptake by plants). Evapoconcentration was suggested as the main mechanism leading to prolonged retention of PFAS in the top 1–2 m of soil.

The main aim of our study is to systematically analyze the effects of root water uptake and nonuniform carbon distribution on PFAS movement in the vadose zone in a temperate humid climate. We performed numerical simulations for two contamination scenarios: leaching of historical contamination and continuous infiltration of contaminated rainwater, with data partly based on the contaminated site in Minnesota described by Xiao et al. (2015). For each scenario, we considered different combinations of root distribution, soil organic carbon distribution, and soil texture.

2. Materials and methods

2.1. Modeling water flow and root water uptake

All numerical simulations were performed with the HYDRUS (Version 5) computer program (Šimůnek et al., 2023, 2024). We assumed that the vertical water flow in the vadose zone can be described by the 1D Richards equation:

$$\frac{\partial \theta(h)}{\partial t} = \frac{\partial}{\partial z}\left[K(h)\left(\frac{\partial h}{\partial z} + 1\right)\right] - S \tag{1}$$

where θ is the volumetric water content (−), t is time (T), z is the vertical coordinate (oriented positively upwards) (L), K is the soil hydraulic conductivity (L T^{-1}), h is the water pressure head (negative in unsaturated conditions) (L), and S is water uptake by plant roots (T^{-1}) (L, T, and M denote the physical dimension of length, time, and mass throughout the text). The soil hydraulic properties are described by the van Genuchten - Mualem model (van Genuchten, 1980; Mualem, 1976):

$$\theta(h) = \theta_r + (\theta_s - \theta_r)\, S_e(h) = \theta_r + (\theta_s - \theta_r)[1 + |\alpha h|^n]^{-m} \tag{2}$$

$$K(h) = K_s\, K_r(S_e(h)) = K_s \sqrt{S_e}\left[1 - \left(1 - S_e^{1/m}\right)^m\right]^2 \tag{3}$$

where S_e is the effective saturation (−), θ_r is the residual water content (−), θ_s is the water content at saturation (−), α (L^{-1}), n (−), m (−) are parameters related to the pore size distribution ($m = 1–1/n$), and K_s is the hydraulic conductivity at saturation (L T^{-1}). Simulations were performed for three soil textures: sand, sandy loam, and loam, using their typical parameters taken from Carsel and Parrish (1988) listed in Table 1.

Water uptake by plant roots is described as:

$$S = a(h)b(z)T_p \tag{4}$$

where a is the water stress response function for plant water uptake (−), b is the normalized root density function (L $^{-1}$), and T_p is the rate of potential transpiration (L T^{-1}) (described later). The stress response function was taken according to the well-known model of Feddes et al. (1978). According to this model $a = 0$ for $h > h_1$ and $h < h_4$, which represents conditions too wet or too dry for plants to extract water. The optimum extraction rate ($a = 1$) occurs between h_2 and h_3 ($h_1 < h_2 < h_3 < h_4$). Linear interpolation of a is applied between h_1 and h_2 and between h_3 and h_4. In our study, we assumed $h_1 = -10$ cm, $h_2 = -25$ cm, $h_3 = -800$ cm, and $h_4 = -8000$ cm, while h_3 varied according to the transpiration rate, with $h_3 = -200$ cm for the rate of 0.5 cm day^{-1} and $h_3 = -800$ cm for the rate of 0.1 cm day^{-1}. These are the default parameters for pasture in HYDRUS 5, based on Wesseling et al. (1991).

The root distribution was taken after Jackson et al. (1996), who proposed a formula describing the average distribution of roots with depth in different biomes based on a compilation of existing literature data:

$$Y(z) = 1 - \beta^{|z|} \tag{5}$$

where $Y(z)$ is the cumulative root fraction ($0 \le Y(z) \le 1$) between the soil surface and depth z (given as a positive number in cm) and β is a parameter depending on the type of biome. We performed simulations for grass (temperate grassland, $\beta = 0.943$) and forest (temperate coniferous forest, $\beta = 0.976$). The corresponding cumulative root distributions are shown in Fig. 1. In both cases, the cumulative root distribution was converted to the root density function $b(z)$ from Eq. (4) by calculating its derivative and normalizing the result so that the integral of $b(z)$

Table 1
Hydraulic parameters for three soil textures (from Carsel and Parrish 1988).

Parameter	Sand	Sandy loam	Loam
θ_s (−)	0.43	0.41	0.43
θ_r (−)	0.045	0.065	0.078
K_s (cm day^{-1})	712.8	106.1	24.96
α (cm^{-1})	0.145	0.075	0.036
n (−)	2.68	1.89	1.56

MOST WIEDZY Downloaded from mostwiedzy.pl

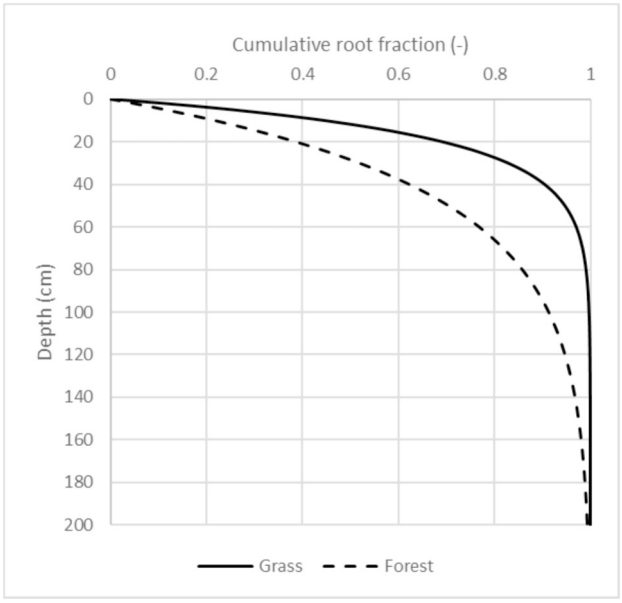

Fig. 1. Distribution of plant roots with depth for grassland and forest (after Jackson et al., 1996).

over the soil profile is equal to 1. Note that $Y(z) < 1$ for all z, i.e. the normalized root density is non-zero everywhere in the profile. However, the cumulative root fraction is equal to 0.9999 at depth of 158 cm for grass and 380 cm for temperate coniferous forest. In our simulations we set the relative density equal to zero below these depths. For comparison, we also performed simulations for bare soil (without roots), as described later.

In all simulations, the bottom boundary condition represented the groundwater table, constant in time ($h = 0$). The profile depth was 2360 cm in the first series of simulations and 1372 cm in the second series of simulations. An atmospheric boundary condition with instantaneous runoff (no ponding) was applied at the soil surface. Depending on the daily weather data, the surface flux switched between infiltration (equal to precipitation) and potential evaporation (E_p), defined as a fraction of potential evapotranspiration (PET). PET was assumed to be equal to the reference evapotranspiration calculated from the Penman-Monteith formula (Allen et al., 1998). PET was split between E_p and T_P (potential transpiration) according to de Beer's law, as implemented in HYDRUS (Šimůnek et al., 2023):

$$E_p = PET\ exp(-k \bullet LAI)\ T_p = PET\ (1 - exp(-k \bullet LAI)) \quad (6)$$

where LAI is the leaf area index (−), and k is the radiation extinction coefficient, taken as 0.463. In the bare soil scenarios, $LAI = 0$ and E_p = PET; thus, the whole potential evapotranspiration flux was assigned as the boundary condition at the surface. For both grass and forest, we assumed $LAI = 2.88$, corresponding to the reference evapotranspiration conditions. In general, LAI depends on plant species and changes during the year. LAI influences the value of PET calculated from Penman-Monteith, as well as its distribution between E_p and T_p via de Beer's law. However, our earlier study (Gumuła-Kawęcka et al., 2022) obtained satisfactory modeling results using LAI values from 2.1 to 2.9 for grassland and a pine forest in a region with a similar climate. While using the same constant value of LAI for both types of plant cover is a simplification of reality, it allows the effects of root distribution on water flow to be separated from the impact of varying potential transpiration.

2.2. Modeling PFAS transport

In this study, we considered two common compounds from the PFAS group: PFOA and PFOS. The movement of each compound in the vadose zone can be described by the following equation (Silva et al., 2020; Guo et al., 2020):

$$\frac{\partial(\theta\, C_w)}{\partial t} + \frac{\partial(\rho_b\, C_s)}{\partial t} + \frac{\partial(A_{aw}\, \Gamma)}{\partial t} = \frac{\partial}{\partial z}\left(\theta\, D \frac{\partial C_w}{\partial z}\right) - \frac{\partial(q\, C_w)}{\partial z} \quad (7)$$

where C_w is the concentration of PFAS in pore water (M L^{-3}), C_s is the concentration of PFAS sorbed on solid phase (−), ρ_b is the dry bulk density of soil (M L^{-3}), Γ is the concentration of PFAS sorbed on AWI (M L^{-2}), A_{aw} is the AWI interfacial area per unit soil volume (L^{-1}), D is the hydrodynamic dispersion coefficient (L^2 T^{-1}), and q is the volumetric water flux (Darcy velocity) (L T^{-1}). The hydrodynamic dispersion coefficient is calculated as $D = \alpha_L\,(q/\theta) + \tau\, D_m$, where α_L is the longitudinal dispersivity [L], q/θ is the pore water velocity, τ is the tortuosity factor for diffusion (−) ($\tau = \theta^{7/3} / \theta_s$), and D_m is the molecular diffusion coefficient for solutes in free water (L^2 T^{-1}) (Table 1). The three terms on the left-hand side represent the change of PFAS mass dissolved in water, sorbed on the solid phase, and sorbed on the AWI, respectively.

Uptake of PFAS by plants was not considered in this study. We considered only water uptake through plant roots to examine the effects of water velocity and water content changes on PFAS movement in the soil profile.

We assumed that the solid phase concentration is related to the concentration in water by a linear isotherm:

$$C_s = K_d\, C_w = f_{oc}\, K_{oc}\, C_w \quad (8)$$

where K_d is the linear distribution coefficient (L^3 M^{-1}), f_{oc} is the fraction of organic carbon in soil (−), and K_{oc} is the partitioning coefficient for a substance in pure organic carbon (L^3 M^{-1}). K_{oc} values are typically determined through laboratory measurements or referenced from available literature. The values used in our study are reported in Table 2. The dry bulk density of soil was assumed to be 1.59 g cm^{-3} in all simulations, following the study of Xiao et al. (2015).

The fraction of organic carbon in soil decreases with depth. Average distributions of soil carbon in the top 3 m of soil were reported by Jobbágy and Jackson (2000) for different biomes. The carbon distributions were provided as a fraction of the total mass of soil carbon in an interval of known soil depths. The intervals allowed for the estimation of f_{oc} distribution in known depths if the value of f_{oc} in the shallow soil layer (0–20 cm) was known. In order to construct a soil profile with a realistic distribution of carbon, we assumed that f_{oc} in the top soil layer up to a 20 cm depth was equal to 1.25 %, as reported by Xiao et al. (2015). We used the OC distribution from Jobbágy and Jackson (2000) to calculate f_{oc} at larger depths.

The distribution of f_{oc} and K_d to the 3 m depth is shown in Table 3, which corresponds to data distribution for temperate grasslands from Jobbágy and Jackson's (2000) study. The SOC distributions reported for temperate forests and bare soils (desert) showed minor differences. For the sake of simplicity and focus on the key priorities of this research, we used the same SOC with all three types of plant cover. Due to a lack of available data for f_{oc} and K_d below the 300 cm depth, we assumed they were constant and the same as in the 200–300 cm interval. For comparison, we also ran a simulation, where we assumed a complete lack of SOC (and sorption only occurred to the AWI) and a constant K_d value (corresponding to the value used throughout the Xiao et al. (2015) study), corresponding to the one from the topmost soil layer (0–20 cm).

Brusseau et al. (2021) demonstrated that depending on measured surface tension and for the PFAS concentrations 3 to 10 times lower than

Table 2
Parameters describing PFAS sorption and diffusion (from Zeng et al., 2021).

Parameter	PFOA	PFOS
K_{oc} (cm^3 g^{-1})	105	617
K_{aw} (cm)	0.0058	0.0427
D_m (cm^2 d^{-1})	0.467	0.467

MOST WIEDZY Downloaded from mostwiedzy.pl

Table 3
Nonuniform distribution of organic carbon in a soil profile.

Depth [cm]	% of the total SOC storage*	f_{oc} [%]	K_d ($cm^3\ g^{-1}$)	
			PFOA	PFOS
0–20	41	1.250	1.309	7.708
20–40	23	0.701	0.734	4.324
40–60	15	0.457	0.479	2.820
60–80	12	0.366	0.383	2.256
80–100	9	0.274	0.287	1.692
100–200	7	0.219	0.229	1.350
200–300	5	0.167	0.175	1.028

* Within the top 3 m of soil.

their critical reference concentrations (as measured by Brusseau and Van Glubt, 2019), the adsorption of contaminants to the air-water interfacial area (AWI) follows a linear process. According to this linear equilibrium model, the PFAS concentration at AWI, Γ, can be determined as:

$$\Gamma = K_{aw}\, C_w \tag{9}$$

where K_{aw} is the coefficient for AWI adsorption in [$cm^3\ cm^{-2}$]. The coefficients for PFOA and PFOS used in our study are given in Table 2. The AWI area is calculated as:

$$A_{aw} = \frac{\rho_w g}{\sigma_0} \int_{\theta_w}^{\theta_s} h(\Theta) d\Theta \tag{10}$$

where ρ_w is the water density ($M\ L^{-3}$), g is the gravitational acceleration ($L\ T^{-2}$), σ_0 is the air-water surface tension ($M\ T^{-2}$), and Θ is an integration variable (−). This approach is implemented in HYDRUS 5, following Bradford and Leij (1997) and Bradford et al. (2015). A_{aw} increases with decreasing water content.

The retardation coefficient R (−) is commonly used to quantify how much the movement of a sorbing contaminant is slowed down compared to a conservative (non-sorbing) contaminant. Assuming linear sorption on the solid phase and AWI, the retardation coefficient can be defined as:

$$R = 1 + \frac{\rho_b K_d}{\theta} + \frac{A_{aw}\, K_{aw}}{\theta} \tag{11}$$

where R can be meaningfully defined when θ, A_{aw}, and the specific discharge q are approximately constant in space and time, i.e., for quasi-steady, uniform flow.

2.3. Simulation setup for leaching of historical PFAS contamination

The first series of simulations was partly based on the data from a contaminated site in Minnesota (USA), described by Xiao et al. (2015). These simulations aimed to show the effects of different assumptions about SOC and root distribution in soil. Only the PFOS movement was considered. The soil profile was homogeneous and consisted of sandy loam. The profile depth was 2360 cm, based on the depth of the water table in the location corresponding to Well #1, which was close to Site 27 and 28, where Xiao et al. (2015) obtained groundwater samples for their study. The profile was uniformly discretized with 937 nodes. The weather data source was the Climate Forecast System Reanalysis (CFSR), accessible as part of the Soil & Water Assessment Tool (SWAT) at https://swat.tamu.edu/data/cfsr. We considered daily weather data from 1979 to 2013 and chose a representative year with precipitation and potential evapotranspiration (PET) close to the average annual values calculated for the entire 35-year period. Out of the 35-year period, the data from 2002 was used since the average potential evapotranspiration (1024 mm/year) and the annual precipitation (903 mm/year) was closest to the average of the 25 years (1022 mm/year and 851 mm/year respectively). The data for the selected year were then repeated 100 times to create a 100-year series of typical weather data used in the simulations. The initial condition for Eq. (1) was obtained by running a warm-up simulation for 100 years, starting from the hydrostatic pressure head distribution above the water table. The final distribution of the water pressure head was used as the initial condition in the actual simulation of the PFOS transport. The initial distribution of PFOS approximated the one shown in Fig. 3 of the paper by Xiao et al. (2015), labeled Site 27. The total PFOS concentration in the soil increased linearly from 0 at the surface to the peak value of 160 ng per gram dry weight (equal to 0.254 μg per cm^3 of soil) at a depth of 68 cm and then decreased linearly to 0 at a depth of 90 cm. In all simulations, the longitudinal dispersivity α_L was equal to 24 cm. This value was used in the study by Zeng et al. (2021), although for a shorter soil profile. Zeng et al. (2021) showed that the choice of α_L significantly influences PFAS movement in the subsurface. However, in this simulation series, we focus on the movement of peak concentration, which is affected mostly by the advection velocity and the retardation factor.

We considered three types of root distributions: bare soil, grass, and forest, and three types of SOC distributions: SOC-0 (no SOC in the soil profile), SOC-V (variable distribution of SOC, decreasing with depth, as described above), and SOC-H (a uniformly high value of SOC, corresponding to the one from the top soil layer, i.e., 1.25 %, as used by Xiao et al., 2015). Altogether, nine simulations were performed to represent PFOS movement for all the possible combinations of the above factors.

2.4. Simulation setup for infiltration of water contaminated with PFAS

In the second simulation series, we investigated the effect of root distribution and soil texture on the movement of PFOA. We considered a homogeneous soil profile with a groundwater table at a depth of 1372 cm. The profile was discretized using 937 nodes, with node spacing of 1 cm in the upper 500 cm of the profile and 2 cm in the lower part. Simulations were performed for 9 cases, i.e., three soil textures: sand (Sa), sandy loam (SaLo), and loam (Lo), and three types of root distributions: bare soil, grass, and forest, as described previously. We used the same realistic SOC distribution in all simulations, with the OC content decreasing with depth (SOC-V), as described earlier. We used daily weather data from January 1, 1979, to July 31, 2014 (12,987 days), taken from the same source as in the first simulation series. In the case of the forest on the loam soil, we had to extend the simulation time by repeating weather data from the earlier period due to the very slow movement of PFOA. The infiltrating water has a constant PFOA concentration of 1 μg cm^{-3}.

At the bottom of the profile, the boundary conditions were $h = 0$ for water flow (a groundwater table, constant in time) and a zero concentration gradient (for PFOA transport). A water flow simulation, starting from the hydrostatic pressure head distribution, was performed using the daily weather data for 35 years to obtain realistic initial conditions for water flow. The final pressure head profile was taken as the starting condition for the actual simulation. The initial PFOA concentration was set to 0 in the whole profile. The longitudinal dispersivity α_L was equal to 63 cm in all simulations (estimated using the formula of Schulze-Makuch, 2005). We compared the results in terms of PFOA concentrations in water, water fluxes, and the cumulative PFOA mass that passed through the depth of 2 m and 6 m in the soil profile.

3. Results and discussion

3.1. Leaching of historical PFAS contamination

Fig. 2 shows the PFOS concentrations in the soil profile after 100 years for all nine scenarios. The position and magnitude of the peak concentration are strongly influenced by the assumed root distribution and SOC distribution. The fastest movement and smallest peak attenuation occur in bare soil, followed by grass and forest. The presence of SOC significantly slows down the movement of PFOS and decreases its peak concentration. Predictably, this retardation effect is much stronger

MOST WIEDZY Downloaded from mostwiedzy.pl

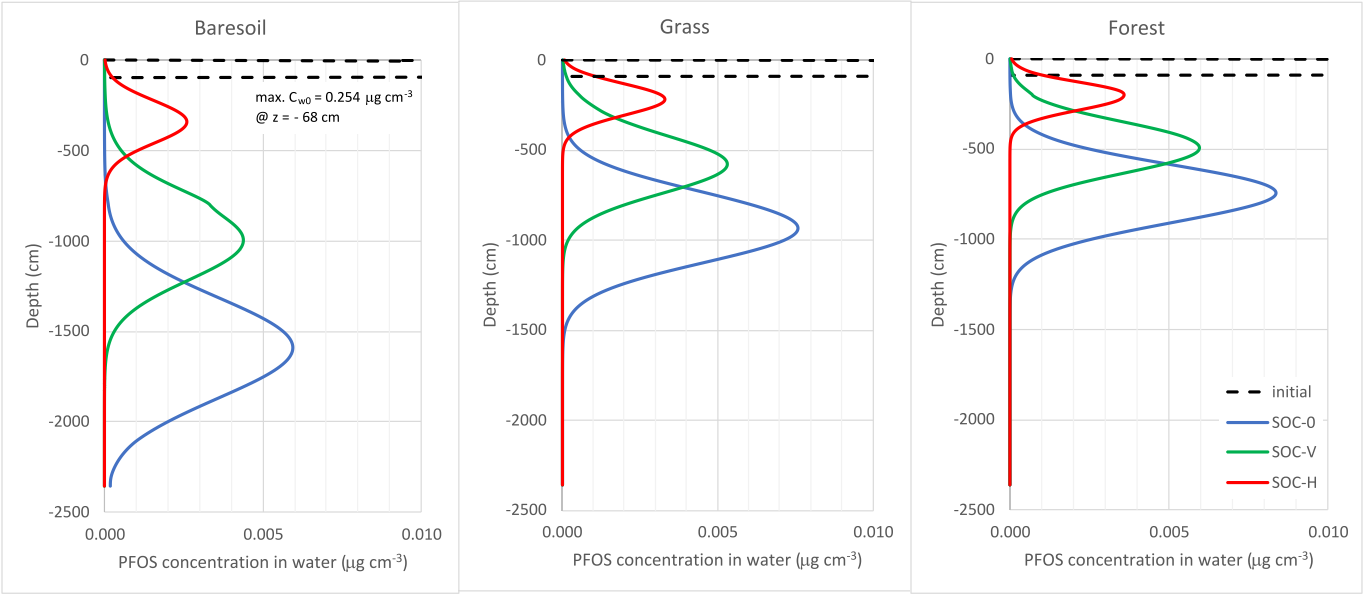

Fig. 2. Profiles of PFOS concentrations in water after 100 years of simulation time in bare soil (left), grassland (middle), and forest (right) (the historical contamination leaching scenario).

in the SOC-H scenarios than in SOC-V. It can be noted that the results for the SOC-V scenarios are quite different from both SOC-H and SOC-0 scenarios.

The distance traveled by the peak concentration in each scenario from the initial position of the peak at a depth of 68 cm is reported in Table 4. For comparison, we also estimate the distance traveled in the same time frame by a conservative (non-sorbing) contaminant. It is calculated as $L = (q/\theta)\, t$, where q is the average unit discharge through the soil profile, θ is the average water content, and $t = 100$ years. The average unit discharge was assumed to equal the average flux reaching the water table at the bottom of the soil profile (groundwater recharge). It equals 42.2 cm yr^{-1} for bare soil, 24.3 cm yr^{-1} for grassland, and 19.0 cm yr^{-1} for forest. Fig. 3 shows the water content changes theta in both space and time. The flow appears quasi-steady and θ does not vary much between the scenarios. We assumed $\theta = 0.15$ to calculate the distances for the conservative contaminant shown in Table 4. This value is in good agreement with Fig. 3. Coincidentally, it is also equal to the value used by Xiao et al. (2015) to estimate the retardation factor in their study, which provided the basis for our numerical simulations.

In Table 4, we also present retardation factors estimated as $R = L_0/L$, where L_0 is the distance traveled by the conservative contaminant, and L is the distance traveled by PFOS for the same root distribution. R differs significantly depending on the SOC distribution. Even for the SOC-0 scenario, we obtained significant retardation factors around 18–19. This is due to the sorption on AWI, which occurs regardless of the assumed SOC distribution. The retardation factor for the SOC-V scenario is more than three times smaller than for SOC-H, which emphasizes the need for realistic data on SOC to predict PFAS fate in the vadose zone. For instance, Xiao et al. (2015) estimated the retardation factor for PFOS as $R = 64$, assuming $\rho_b = 1.59$ g/cm3, $\theta = 0.15$, $f_{oc} = 1.25$ % in the topsoil (the same as in our study) and $K_{oc} = 479$ cm^3 g^{-1} (less than in our study). Moreover, they neglected AWI sorption in the calculation of R. Our estimate of R with a realistic SOC distribution varies between 29 and 32 (Table 1), about two times less than in Xiao et al. (2015), despite the presence of AWI sorption. Without AWI sorption, the R factor for the SOC-V scenario would be only about 11 to 13 (the difference between R for SOC-V and SOC-0 in Table 4 plus one). Based on our simulation results, for SOC-H without AWI sorption, one would obtain R around 78 to 88, somewhat larger than 64 reported by Xiao et al. (2015), due to the larger K_{oc} used in our study.

The retardation factors calculated from the travel distance of the peak concentration in the numerical solution are in good agreement with the estimates from Eq. (11) for those scenarios where f_{oc} and K_d are uniform, i.e., for SOC-0 and SOC-H. The evolution of the AWI area within a single year for different scenarios is shown in Fig. 3. Note that the same pattern repeats each year because of the repeating set of yearly weather data. Significant temporal changes in the AWI area are visible only in the scenarios with the root zone in the uppermost part of the profile, where θ decreases and A_{aw} increases due to increased evapotranspiration in summer. Taking approximately $A_{aw} = 70$ cm^{-1}, which is representative of the deeper vadose zone, we obtain from Eq. (11) $R = 20.9$ for $\theta = 0.15$ and $K_d = 0$ (SOC-0) and $R = 102.5$ for $K_d = 7.7$ cm^3 g^{-1} (SOC-H). These estimates are reasonably close to the values in Table 1 because the parameters involved in Eq. (1) do not change significantly in space and time. However, estimating K_d that should be used in Eq. (1) for the SOC-V scenario is challenging, as K_d varies with depth. The average K_d can be back-calculated from Eq. (1), assuming that (without AWI) $R = 1 + \rho_b K_d/\theta$ should be approximately equal to 12 (see above). The resulting K_d is 1.04 cm^3 g^{-1}, i.e., very close to the minimum K_d value applied in the soil profile below the depth of 200 cm. Thus, the long-

Table 4
Travel distances of the peak concentration in 100 years and retardation factors calculated for different scenarios of historical contamination leaching.

Scenario	Bare soil		Grass		Forest	
	Distance (cm)	R (–)	Distance (cm)	R (–)	Distance (cm)	R (–)
Conservative	28,122	1.00	16,196	1.00	12,685	1.00
SOC-0	1523	18.46	865	18.72	676	18.76
SOC-V	930	30.24	509	31.82	426	29.78
SOC-H	275	102.26	151	107.26	131	96.83

MOST WIEDZY Downloaded from mostwiedzy.pl

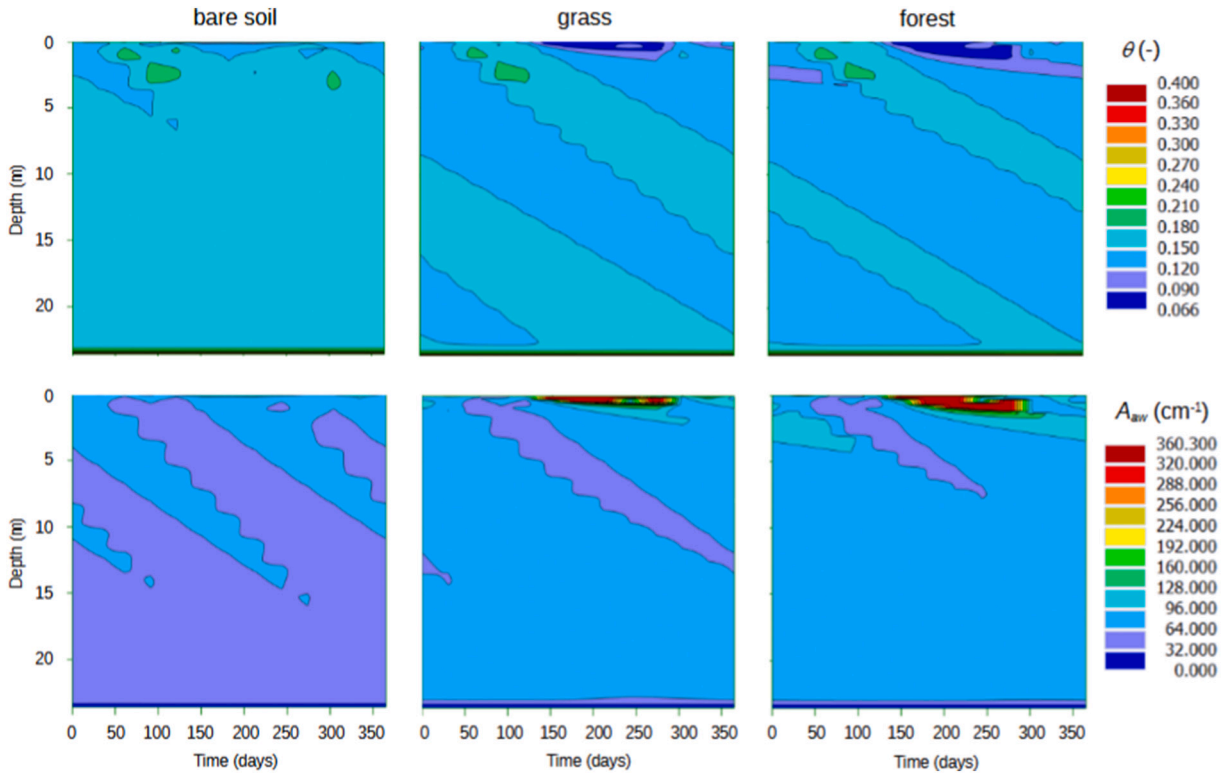

Fig. 3. Evolution of the volumetric water content (top) and AWI area (bottom) in bare soil (left), grassland (middle), and forest (right) during a single year in the simulation of historical PFOS contamination leaching.

term fate of PFAS in the deep vadose zone is not significantly influenced by the increased organic carbon content of the soil close to the surface. We should note that in real settings, the carbon content in the deep vadose zone is probably even lower than 0.167 %, as used here. Again, this shows that realistic estimates of SOC in deeper soil horizons are of paramount importance for PFAS modeling.

The assumptions regarding root distribution also significantly influence the predictions of PFOS movement. Fig. 3 shows that the presence of roots clearly increases the AWI area in the root zone because the water content is reduced due to water uptake by plants. Thus, one could expect enhanced sorption of PFOS on AWI in the scenarios with plant cover. However, as shown in Table 4, all retardation factors, including those related to AWI sorption only (the SOC-0 scenario), are quite similar for each type of root distribution. It seems that, similarly to the increased SOC, the larger A_{aw} due to transpiration in the upper soil layers does not significantly affect the long-term movement of PFAS. The main mechanism by which the roots influence PFAS movement seems to be the reduction in the downward water flux due to increased evapotranspiration. Using data from Table 1, we can calculate an apparent retardation factor due to the presence of root zone as $R_r = L_B / L$, where L_B is the distance traveled by the peak concentration in the bare soil profile, and L is the corresponding distance in a profile with vegetation. R_r was found to be quite similar for each SOC distribution, ranging from 1.76 to 1.83 for grass and from 2.10 to 2.25 for forest. These numbers closely match the corresponding ratios of the groundwater recharge rates, which are 1.74 (bare soil/grass) and 2.22 (bare soil/forest). A similar effect of slowing the downward movement due to the root zone was also shown for conservative contaminants (e.g., Szymkiewicz et al., 2018, 2019).

3.2. Infiltration of water contaminated with PFAS

The results of simulations are shown in Figs. 4 and 5 for the depths 2 and 6 m, respectively. The breakthrough curves for PFOA concentrations show oscillations, with magnitudes depending on the soil type and root distribution. We note that these changes are related to the dynamic nature of the AWI area, which dramatically changes with changes in water contents under transient water flow conditions, dynamically altering the AWI sorption capacity. This is contrary to sorption to the solid phase, which is constant (proportional to the soil bulk density) and independent of transient flow conditions. The oscillations in the sand are relatively small, and quasi-steady conditions are reached at both 2 m and 6 m depths. The average concentration in the quasi-steady phase is larger than in the infiltrating water: around 1.4 mg/cm^3 for bare soil, 2.2 mg/cm^3 for grass, and 2.7 mg/cm^3 for forest. The PFOA concentration in water increases due to evapotranspiration, which takes out some of the water and reduces the downward flux without decreasing the mass of dissolved PFAS. This effect is more pronounced for grass and forest than for bare soil since the presence of the root zone increases actual evapotranspiration. Moreover, the increase in concentration is more significant fine textured soils. In Fig. 4 the maximum PFOA concentrations in pore water are higher in sandy loam (around 5 μg cm^{-3}) and loam (around 7 μg/cm^{-3}) than in sand (around 3 μg/cm^{-3}). The increase of PFAS concentration due to evapotranspiration can be called evapo-concentration, following Wallis et al. (2022). However, our simulations were performed for a humid climate with general excess of infiltration over evapotranspiration and the upward water fluxes in soil were negligible, as shown in Figs. 4 and 5. In contrast, the study of Wallis et al. (2022) focused on a more arid climate, where the upward movement of water with dissolved PFAS significantly contributed to increased concentrations in top soil.

The oscillations in PFOA concentrations seen in Figs, 4 and 5 are related to the seasonal changes in water contents, leading to changes in AWI areas. In sandy loam and loam, the changes in water contents and AWI are much larger than in sand (Fig. 6), causing larger oscillation amplitudes in the PFOA concentrations. The maximum PFOA concentrations in loam reach up to 7 mg/cm^3 for the forest. Also, the steady state is not reached in loam even at the end of simulation time because

MOST WIEDZY Downloaded from mostwiedzy.pl

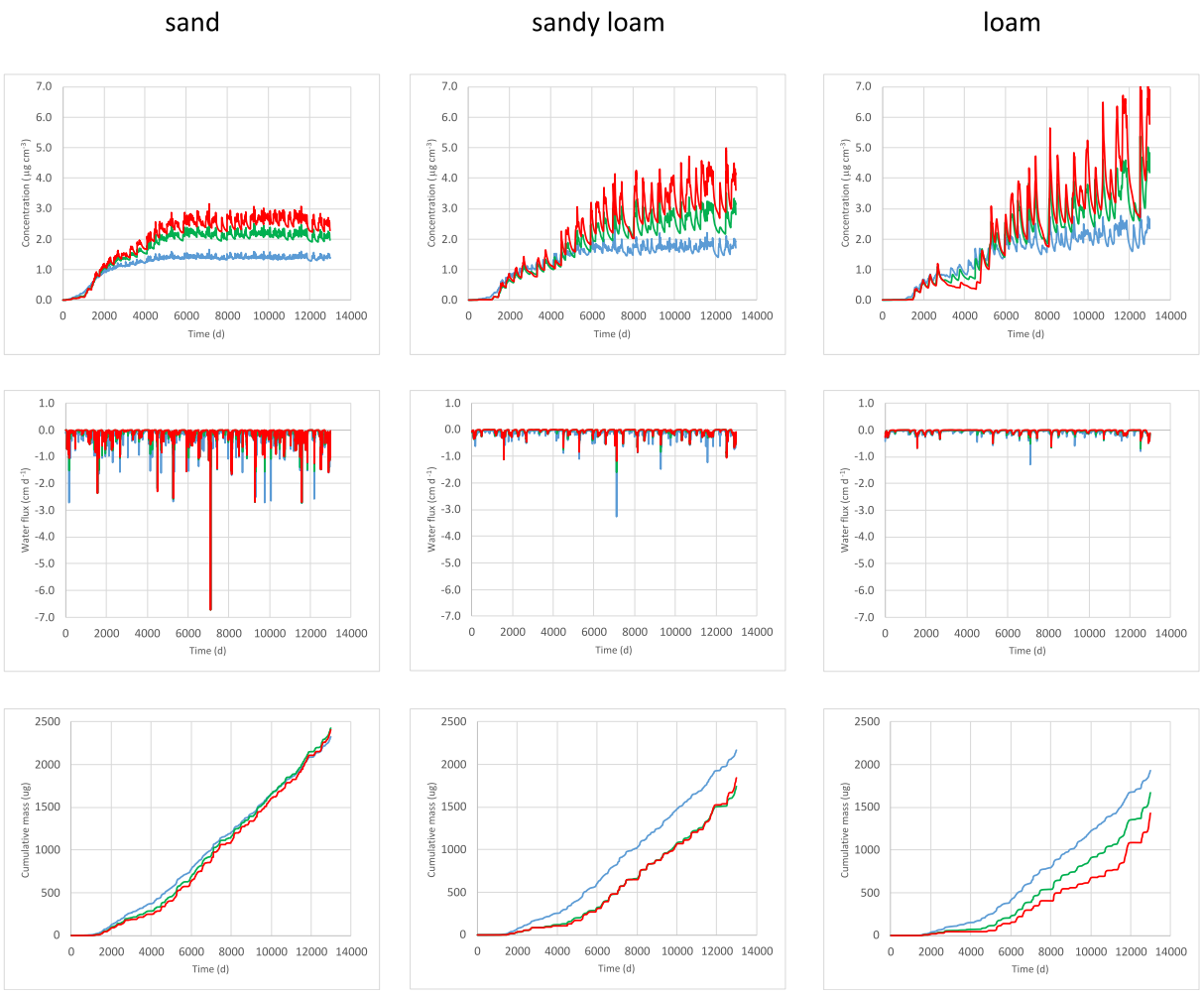

Fig. 4. PFOA concentrations in water (top), water fluxes (middle), and cumulative PFOS mass fluxes (bottom) at a depth of 2 m in sandy (left), sandy loam (middle) and loam (right) soil profile in the simulations representing infiltration of contaminated water. Results for different root distributions are distinguished by colors (blue – bare soil, green – grass, red – forest).

the flow and transport processes are much slower than in sand or sandy loam. The decrease in water content during dry months lead to counteracting effects on PFAS concentrations. On the one hand, a decrease in water content without a loss of PFOA and PFOS should lead to higher concentration in the bulk soil. On the other hand, an increase in AWI leads to lower concentration in the water phase.

The variability of weather conditions between subsequent years also influences the results. For example, in Fig. 4, in the loam-forest scenario, a significant decrease in concentrations is observed approximately between day 3000 and 4500. Fig. 4 shows that this is a dry period with almost no flow in the soil profile. On the other hand, we can see in Fig. 6 that in the corresponding time period, the water content is reduced, and the AWI area increased in the part of the loam profile around 2 m deep, leading to enhanced sorption of PFOA on AWI. Note that a different color scale is used for the AWI area in Fig. 6 for the loam and sand profiles. The maximum A_{aw} in sand during the whole simulation is 67.11 cm^{-1}, while in loam, it is 2059 cm^{-1}.

Since concentrations and water fluxes vary significantly with time, an analysis of concentration evolution is insufficient to quantify the slowdown of contaminant movement due to the presence of roots. In this context, the plots of the cumulative PFOA mass passing through a specific depth are more helpful (shown in the bottom rows of Figs. 4 and 5). While PFOA transport in profiles with root zones is always slower than in the bare soil profile, the difference depends strongly on the soil texture and depth and varies with time. For example, choosing arbitrarily the characteristic time corresponding to the cumulative mass equal to 500 µg, we obtain the ratios of times between forest and bare soils given in Table 5 (for loam, we had to extend the simulation period; the results are not shown in Fig. 5). The ratios are clearly larger for finer textures (sandy loam and loam) than for sand, and they increase with depth for all soil textures.

3.3. Limitations of the analysis

The presented results were obtained using several simplifying assumptions, which must be clearly understood. We focused on two common PFAS compounds: PFOS and PFOA. However, although field data show that these compounds are the most frequently tested PFAS, other species are present in contaminated zones (e.g., Johnson, 2022; Batayi et al., 2021; Silva et al., 2022). Since the PFAS group expanded from 9000 to 15,000 compounds (US EPA, 2021) just during this research, many more compounds should be considered when determining the real soil and water concentrations of these pollutants. Furthermore, we assumed a simplified description of PFAS sorption on AWI and SOC using linear models. AWI area was calculated using the thermodynamic approach, which may underestimate the extent of sorption, especially in dry conditions (Brusseau, 2023). Furthermore, solid sorption was related only to SOC, while it may also occur on clay minerals and metal oxides (e.g. Zeng and Guo, 2023). We are also aware that PFAS could be absorbed by plants and adsorbed to plant roots.

MOST WIEDZY Downloaded from mostwiedzy.pl

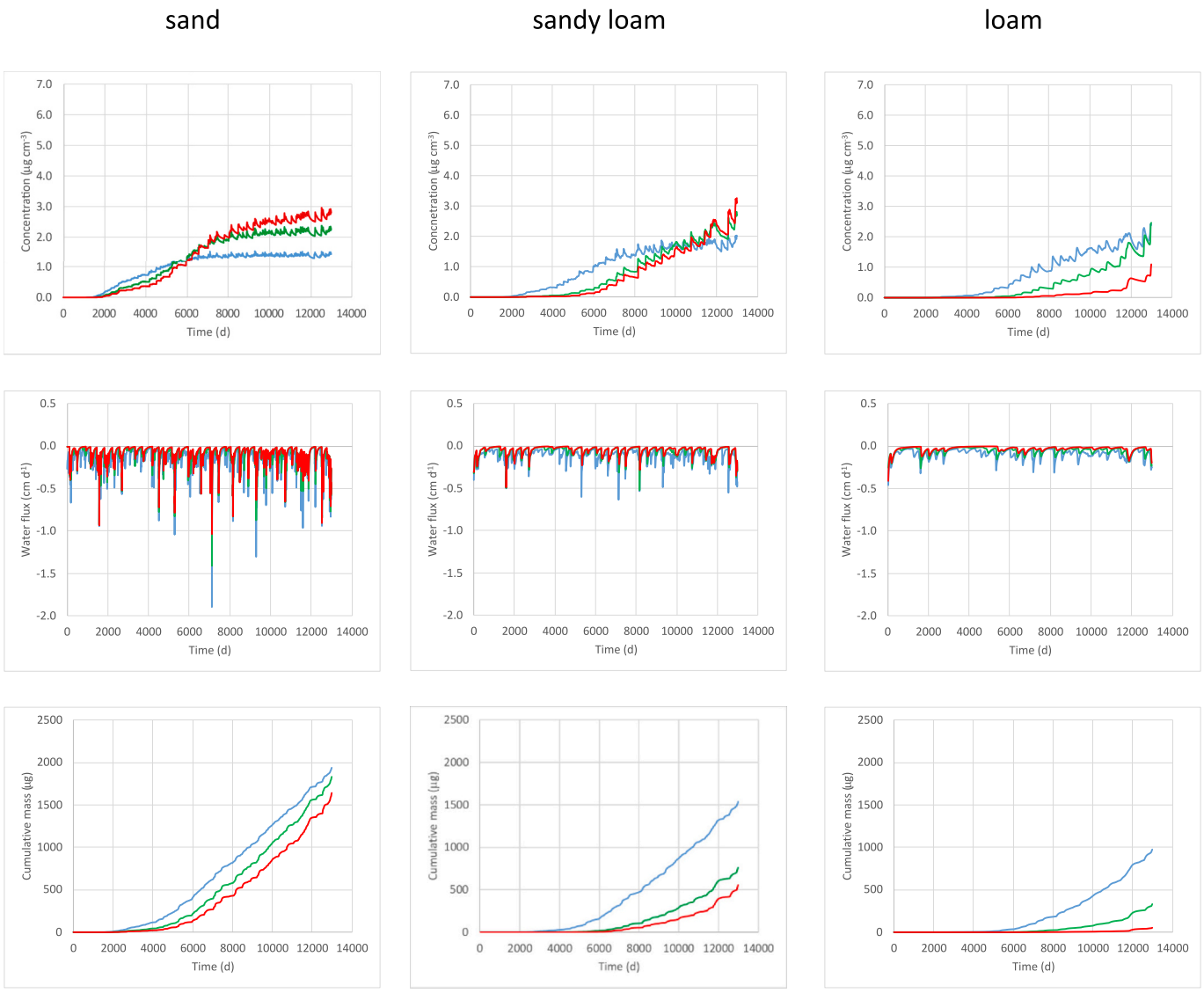

Fig. 5. PFOA concentrations in water (top), water fluxes (middle), and cumulative PFOS mass fluxes (bottom) at a depth of 6 m in sandy (left), sandy loam (middle) and loam (right) soil profile in the simulations representing infiltration of contaminated water. Results for different root distributions are distinguished by colors (blue – bare soil, green – grass, red – forest).

However, only limited data on this factor are currently available and vary depending on the type of plant species and PFAS, as well as infiltrating concentrations (Held and Reinhard, 2020; Felizeter et al., 2021; Xu et al., 2022; Blaine et al., 2014). Therefore, we could not incorporate this factor into our study due to insufficient data.

For simulation models using data from temperate grasslands and temperate coniferous forests, the average constant for a variety of species present in these biomes was used (Jackson et al., 1996), rather than accounting for the diversity of species present, which would be a more realistic representation. Also, we did not consider seasonal or long-term root growth or the LAI changes affecting evapotranspiration.

We considered only homogeneous soil profiles, while it has been shown that soil heterogeneity influences PFAS movement. For instance, Silva et al. (2022) found that the impact of AWI adsorption was more significant for PFAS transport within homogeneous soils than texturally heterogeneous soils considered in their study. Zeng and Guo (2021, 2023) used a 3D model to show the importance of preferential flow paths and capillary barriers on PFAS spreading in the subsurface. They concluded that soil heterogeneities are among the primary sources of uncertainty for predicting PFAS leaching and retention in the vadose zone. The interplay between water uptake by roots and soil heterogeneities was outside the scope of this study and remains to be investigated.

In both series of simulations, the groundwater table was relatively deep and constant in time. Groundwater table fluctuations can be expected to affect PFAS fate by creating or destroying AWI during the transition from unsaturated to saturated conditions and vice versa. The weather conditions used to run the first series of simulations were obtained by selecting a yearly data set from the 35-year period to depict the average conditions. The limitation of using this data is that it neglects climate change and fluctuating weather patterns such as wet or dry periods. The second series of simulations showed the influence of year-to-year variations in weather conditions.

4. Conclusions

In this study, we investigated the effect of soil organic carbon distribution and water uptake by plant roots on PFAS movement in the vadose zone with a deep groundwater table under temperate, humid climate conditions. We found that both SOC distribution and root zone significantly affect PFAS transport.

The apparent retardation factor for realistic SOC distribution was

MOST WIEDZY Downloaded from mostwiedzy.pl

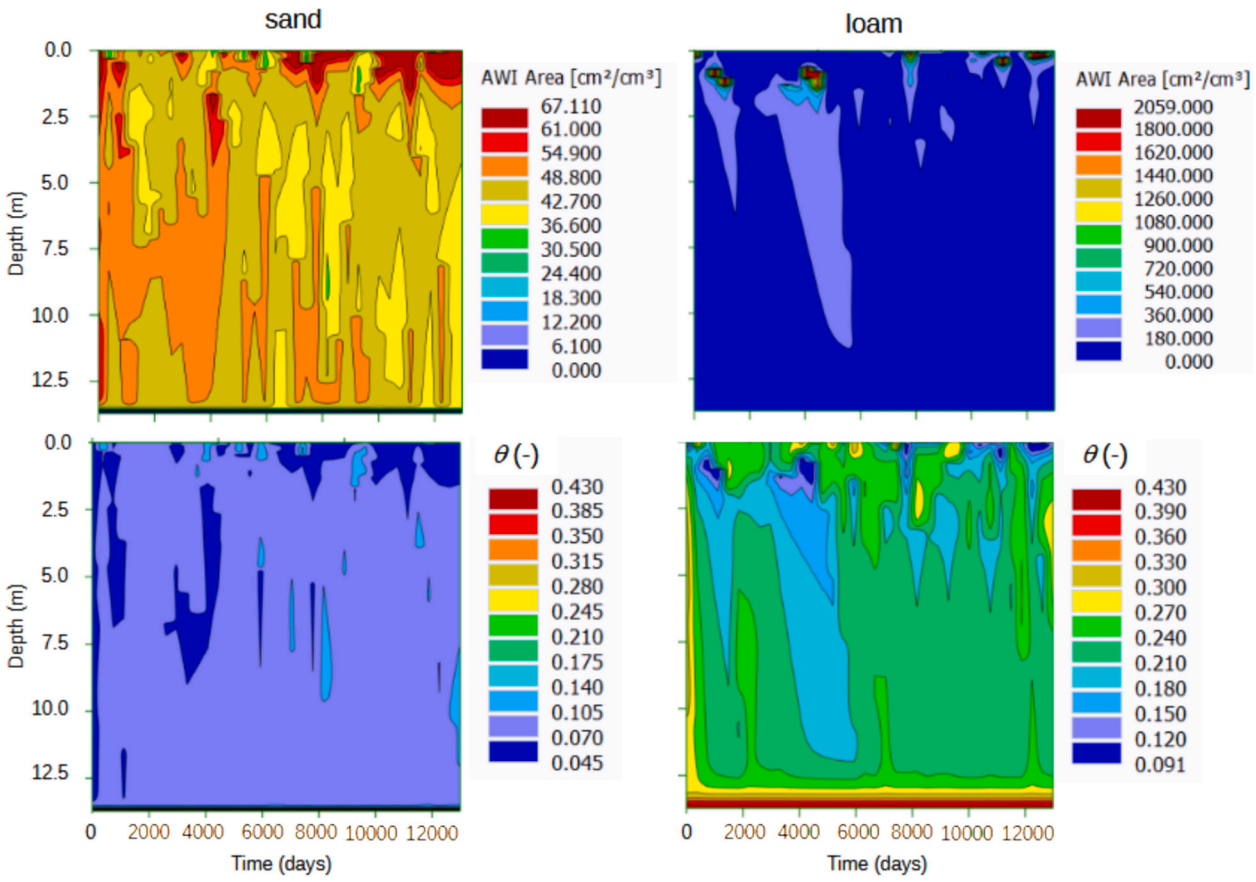

Fig. 6. AWI areas (top) and water contents (bottom) as a function of depth and time during the simulations representing infiltration of contaminated water in the sandy (left) and loamy (right) forest profiles.

Table 5
Ratios between the characteristic times for forest and bare soils. The characteristic time corresponds to when the cumulative leaching mass at a particular depth of 500 μg is reached, as shown in Figs. 4 and 5.

Soil texture	Depth 2 m	Depth 6 m
Sand	1.13	1.28
Sandy loam	1.32	1.58
Loam	1.34	1.54

twice as large as for the scenario with no SOC (only AWI sorption) and more than three times smaller than for the scenario with a uniformly high SOC content, equal to the content in topsoil. Thus, realistic SOC distribution must be considered when predicting PFAS fate in soils and groundwater vulnerability to contamination. Using SOC estimates based on sampling shallow soil layers overestimates PFAS travel times significantly.

We also showed that the root distribution in soil profoundly impacts the simulations of PFAS migration through soil. The presence of the root zone slows the movement of PFAS significantly, primarily due to increased evapotranspiration and reduced downward water flux. Another effect of water uptake by plant roots is an increase in PFAS concentrations in soil water, i.e. evapo-concentration, shown earlier by Wallis et al. (2022) for a more arid climate. In our simulations, significant evapo-concentration was observed in a temperate humid climate. PFAS concentrations changed seasonally with varying soil water contents. They were also influenced by year-to-year variability in precipitation. The evapo-concentration and the slowdown of PFAS movement due to root water uptake are more significant in fine-textured soils than in sand. Our work extended the analysis of Wallis et al. (2022) by considering various soil textures and SOC distributions and focusing on a different climate.

Despite several simplifying assumptions, our study highlights the importance of using realistic data about the distribution of soil organic carbon and plant roots for accurate predictions of PFAS fate in the subsurface. Further research is needed to investigate the role of additional factors such as soil heterogeneity, groundwater table fluctuations, and climate change.

CRediT authorship contribution statement

Barbara Jennifer Biesek: Writing – original draft, Visualization, Investigation, Formal analysis, Data curation, Conceptualization. **Adam Szymkiewicz:** Writing – review & editing, Supervision, Methodology, Investigation, Conceptualization. **Jirka Šimůnek:** Writing – review & editing, Software. **Anna Gumuła-Kawęcka:** Investigation. **Beata Jaworska-Szulc:** Investigation.

Declaration of competing interest

The authors declare that they have no known competing financial interests or personal relationships that could have appeared to influence the work reported in this paper.

Data availability

Data will be made available on request.

MOST WIEDZY Downloaded from mostwiedzy.pl

References

Allen, R.G., Pereira, L.S., Raes, D., Smith, M., 1998. Crop evapotranspiration-guidelines for computing crop water requirements-FAO irrigation and drainage paper 56. Fao, Rome 300 (9), D05109.

Anderson, R.H., 2021. The case for direct measures of soil-to-groundwater contaminant mass discharge at AFFF-impacted sites. Environ. Sci. Technol. 55 (10), 6580–6583.

Batayi, B., Okonkwo, O., Daso, A.P., 2021. Poly- and perfluorinated substances in environmental water from the Hartbeespoort and Roodeplaat Dams, South Africa. Water SA 47. https://doi.org/10.17159/wsa/2021.v47.i1.9445.

Blaine, A., Rich, C., Sedlacko, E., Hyland, K., Stushnoff, C., Dickenson, E., Higgins, C., 2014. Perfluoroalkyl acid uptake in lettuce (*Lactuca sativa*) and strawberry (*Fragaria ananassa*) irrigated with reclaimed water. Environ. Sci. Technol. 48 https://doi.org/10.1021/es504150h.

Bradford, S.A., Leij, F.J., 1997. Estimating interfacial areas for multi-fluid soil systems. J. Contam. Hydrol. 27, 83–106.

Bradford, S.A., Wang, Y., Torkzaban, S., Šimůnek, J., 2015. Modeling the release of E. Coli D21g with transients in water content. Water Resour. Res. 51, 3303–3316.

Brusseau, M., Van Glubt, S., 2019. The influence of surfactant and solution composition on PFAS adsorption at fluid-fluid interfaces. Water Res. 161 https://doi.org/10.1016/j.watres.2019.05.095.

Brusseau, M.L., 2023. Determining air-water interfacial areas for the retention and transport of PFAS and other interfacially active solutes in unsaturated porous media. Sci. Total Environ. 884, 163730.

Brusseau, M.L., Guo, B., 2021. Air-water interfacial areas relevant for transport of per and poly-fluoroalkyl substances. Water Res. 207, 117785.

Brusseau, M.L., Guo, B., Huang, D., Yan, N., Lyu, Y., 2021. Ideal versus nonideal transport of PFAS in unsaturated porous media. Water Res. 202, 117405.

Carsel, R.F., Parrish, R.S., 1988. Developing joint probability distributions of soil water retention characteristics. Water Resour. Res. 24, 755–769.

Feddes, R.A., Kowalik, P.J., Zaradny, H., 1978. Simulation of field water use and crop yield. Simul. Monogr. PUDOC.

Felizeter, S., Juerling, H., Kotthoff, M., De Voogt, P., McLachlan, M., 2021. Uptake of perfluorinated alkyl acids by crops: results from a field study. Environ Sci Process Impacts 23. https://doi.org/10.1039/D1EM00166C.

van Genuchten, M.Th., 1980. A closed-form equation for predicting the hydraulic conductivity of unsaturated soils. Soil Sci. Soc. Am. J. 44, 892–898.

Gumuła-Kawęcka, A., Jaworska-Szulc, B., Szymkiewicz, A., Gorczewska-Langner, W., Pruszkowska-Caceres, M., Angulo-Jaramillo, R., Simunek, J., 2022. Estimation of groundwater recharge in a shallow sandy aquifer using unsaturated zone modeling and water table fluctuation method. J. Hydrol. 605, 127283 https://doi.org/10.1016/j.jhydrol.2021.127283.

Guo, B., Zeng, J., Brusseau, M.L., 2020. A mathematical model for the release, transport, and retention of per- and polyfluoroalkyl substances (PFAS) in the vadose zone. Water Resour. Res. 56 (2), e2019WR026667.

Guo, B., Zeng, J., Brusseau, M.L., Zhang, Y., 2022. A screening model for quantifying PFAS leaching in the vadose zone and mass discharge to groundwater. Adv. Water Resour. 160, 104102.

Held, T., Reinhard, M., 2020. Project No. (FKZ) 3717 76 231 0. Report No. FB000332/ENG. Remediation management for local and widespread PFAS contaminations.

Hutson, J.L., 2003. LEACHM: Leaching Estimation and Chemistry Model; a Process-Based Model of Water and Solute Movement, Transformations, Plant Uptake and Chemical Reactions in the Unsaturated Zone; Version 4. Cornell Univ, Ithaca.

Jackson, R.B., Canadell, J., Ehleringer, J.R., Mooney, H.A., Sala, O.E., Schulze, E.D., 1996. A global analysis of root distributions for terrestrial biomes. Oecologia 108 (3), 389–411.

Jobbágy, E.G., Jackson, R.B., 2000. The vertical distribution of soil organic carbon and its relation to climate and vegetation. Ecol. Appl. 10 (2), 423–436.

Johnson, G., 2022. PFAS in soil and groundwater following historical land application of biosolids. Water Res. 211, 118035 https://doi.org/10.1016/j.watres.2021.118035.

Li, Y., Oliver, D.P., Kookana, R.S., 2018. A critical analysis of published data to discern the role of soil and sediment properties in determining sorption of per and polyfluoroalkyl substances (PFASs). Sci. Total Environ. 628, 110–120.

Minnesota Pollution Control Agency, 2024. Minnesota Department of Health, DNR & MDA. Authors Greene S. & Neuschler C. (Published February 2021). Minnesota's PFAS Blueprint. Document number: p-gen1–22 Accessed on Jan 19th. https://www.pca.state.mn.us/sites/default/files/p-gen1-22.pdf.

Mualem, Y., 1976. A new model for predicting the hydraulic conductivity of unsaturated porous media. Water Resour. Res. 12 (3), 513–522.

Murphy, C., Schaffrath, C., O'Hagan, D., 2003. Fluorinated natural products: the biosynthesis of fluoroacetate and 4-fluorothreonine in Streptomyces cattleya. Chemosphere 52, 455–461. https://doi.org/10.1016/S0045-6535(03)00191-7.

Nguyen, T.M.H., Bräunig, J., Thompson, K., Thompson, J., Kabiri, S., Navarro, D.A., Mueller, J.F., 2020. Influences of chemical properties, soil properties, and solution pH on soil–water partitioning coefficients of per-and polyfluoroalkyl substances (PFASs). Environ. Sci. Technol. 54 (24), 15883–15892.

Schulze-Makuch, D., 2005. Longitudinal dispersivity data and implications for scaling behavior. Groundwater 43 (3), 443–456.

Sharifan, H., Bagheri, M., Wang, D., Burken, J.G., Higgins, C.P., Liang, Y., Liu, J., Schaefer, C., Blotevogel, J., 2021. Fate and transport of per-and polyfluoroalkyl substances (PFASs) in the vadose zone. Sci. Total Environ. 771, 145427.

Silva, J.A., Guelfo, J.L., Šimůnek, J., McCray, J.E., 2022. Simulated leaching of PFAS from land-applied municipal biosolids at agricultural sites. J. Contam. Hydrol. 251, 104089.

Silva, J.A.K., Šimůnek, J., McCray, J.E., 2020. A modified HYDRUS model for simulating PFAS transport in the vadose zone. Water 12 (10), 2758.

Šimůnek, J., van Genuchten, M.T., Šejna, M., 2008. Development and applications of the HYDRUS and STANMOD software packages and related codes. Vadose Zone J. 7 (2), 587–600.

Šimůnek, J., van Genuchten, M.T., Šejna, M., 2023. The HYDRUS Software Package for Simulating the One-, Two-, and Three-Dimensional Movement of Water, Heat, and Multiple Solutes in Variably-Saturated Porous Media. Technical Manual II. HYDRUS 2D/3D. ver. 5.xx.

Šimůnek, J., Brunetti, G., Jacques, D., van Genuchten, M.Th., Šejna, M., 2024. Recent developments and applications of the HYDRUS computer software packages since 2016, a special issue tribute to Rien van Genuchten, recipient of the 2023 wolf prize for agriculture. Vadose Zone J. https://doi.org/10.1002/vzj2.20310 accepted January 2, 2024.

Smith, J., Brusseau, M.L., Guo, B., 2024. An integrated analytical modeling framework for determining site-specific soil screening levels for PFAS. Water Res. 252, 121236.

Szymkiewicz, A., Gumuła-Kawęcka, A., Potrykus, D., Jaworska-Szulc, B., Pruszkowska-Caceres, M., Gorczewska-Langner, W., 2018. Estimation of conservative contaminant travel time through vadose zone based on transient and steady flow approaches. Water 10 (10), 1417.

Szymkiewicz, A., Savard, J., Jaworska-Szulc, B., 2019. Numerical analysis of recharge rates and contaminant travel time in layered unsaturated soils. Water 11 (3), 545.

United States Environmental Protection Agency, 2021. EPA 822-F-21-007. Technical Fact Sheet: Human Health Toxicity Assessment for GenX Chemicals. Table 2. Comparison of Chronic Toxicity Values for the Four PFAS with Final EPA Toxicity Assessments. Retrieved August 19, 2022 from. https://www.epa.gov/system/files/documents/2021-10/genx-final-tox-assess-tech-factsheet-2021.pdf.

United States Environmental Protection Agency, 2024. Comptox Chemicals Dashboard: Master List of PFAS Substances (Version 2). Retrieved Jan 13, 2024 from. https://comptox.epa.gov/dashboard/chemical_lists/pfasmaster.

Vahedian, F., Silva, J.A.K., Šimůnek, J., McCray, J.E., 2024. The influence of tension-driven flow on the transport of AFFF in unsaturated media. ACS ES&T Water 11. https://doi.org/10.1021/acsestwater.3c00611.

Wallis, I., Hutson, J., Davis, G., Kookana, R., Rayner, J., Prommer, H., 2022. Model-based identification of vadose zone controls on PFAS mobility under semi-arid climate conditions. Water Res. 225, 119096.

Wesseling, J.G., Elbers, J.A., Kabat, P., van den Broek, B.J., 1991. SWATRE: Instructions for Input, Internal Note. Winand Staring Centre, Wageningen, the Netherlands.

Xiao, F., Simcik, M.F., Halbach, T.R., Gulliver, J.S., 2015. Perfluorooctane sulfonate (PFOS) and perfluorooctanoate (PFOA) in soils and groundwater of a US metropolitan area: migration and implications for human exposure. Water Res. 72, 64–74.

Xu, B., Qiu, W., Du, J., Wan, Z., Zhou, J.L., Chen, H., Liu, R., Magnuson, J.T., Zheng, C., 2022. Translocation, bioaccumulation, and distribution of perfluoroalkyl and polyfluoroalkyl substances (PFASs) in plants. iScience Mar 11;25 (4), 104061. https://doi.org/10.1016/j.isci.2022.104061. PMID: 35345465; PMCID: PMC8957016.

Zeng, J., Guo, B., 2021. Multidimensional simulation of PFAS transport and leaching in the vadose zone: impact of surfactant-induced flow and subsurface heterogeneities. Adv. Water Resour. 155, 104015.

Zeng, J., Guo, B., 2023. Reduced accessible air–water interfacial area accelerates PFAS leaching in heterogeneous vadose zones. Geophys. Res. Lett. 50 (8), e2022GL102655.

Zeng, J., Brusseau, M.L., Guo, B., 2021. Model validation and analyses of parameter sensitivity and uncertainty for modeling long-term retention and leaching of PFAS in the vadose zone. J. Hydrol. 603, 127172.

MOST WIEDZY Downloaded from mostwiedzy.pl